

## Current-voltage characteristics of silicon solar cells: Determination of base doping concentration and hysteresis correction

Tobias Kemmer\*, Johannes M. Greulich, Alexander Krieg, Stefan Rein

Fraunhofer Institut für Solar Energy Systems ISE, Heidenhofstr. 2, 79110, Freiburg, Germany



### ARTICLE INFO

**Keywords:**  
Hysteresis  
Transient-error  
Capacitance-effect  
Current-voltage characterization  
Base doping concentration

### ABSTRACT

The measurement of the current-voltage (*IV*) characteristics is the most important step for quality control and optimization of the fabrication process in research and industrial production of silicon solar cells. The occurrence of transient errors and hysteresis effects in *IV*-measurements can hamper the direct analysis of the *IV*-data of high-capacitance silicon solar cells. We propose a novel procedure to reconstruct a quasi-steady-state (qss) *IV*-characteristics from hysteretic measurements by aligning the generalized current density of forward and backward sweeps. In the process, the base doping concentration  $N_B$  and the cell thickness  $d$  are used as optimization parameters and calculated alongside the qss-*IV*-curve. We summarize the theory behind the method, describe the experimental implementation and verify the applicability of the approach by comparing the extracted doping concentration to multiple alternative methods. For a test set of more than 100 silicon heterojunction solar cells with doping concentrations between 3 and  $7 \cdot 10^{15} \text{ cm}^{-3}$  a RMSD  $< 3.4 \cdot 10^{14} \text{ cm}^{-3}$  is achieved. Basic parameter extraction from the qss-*IV*-curve closely match reference values with a RMSD  $< 0.1 \%_{\text{abs}}$  in efficiency and fill factor.

### 1. Introduction

The current-voltage (*IV*) characteristics is one of the most important measurements in the analysis of solar cells in both, research and industrial mass production. It allows the extraction of central performance indicators such as efficiency  $\eta$ , fill factor  $FF$ , maximum power  $P_{\max}$ , short-circuit current  $I_{sc}$  and open-circuit voltage  $V_{oc}$ . To satisfy the increasing demand for solar cells, the throughput of solar cell production lines increases continuously. To further increase the throughput, the voltage sweep duration during *IV*-characterization is desired to be as short as possible.

At the same time, improvements in material quality and passivation technology have led to increased minority carrier lifetimes and thus an increase of the internal cell-capacitance  $C$  [1]. This effect is especially pronounced in solar cells with high base resistivity, high efficiency and high  $V_{oc}$  [1], e.g. in silicon heterojunction (SHJ) solar cells [2]. The combination of reduced measurement duration and increased minority carrier lifetimes, both quantities being in the same order of magnitude, leads to increasing transient errors in the form of hysteresis, when measuring from  $I_{sc}$  to  $V_{oc}$  (forward, fw) and from  $V_{oc}$  to  $I_{sc}$  (backward, bw). As a result,  $V_{oc}$ ,  $FF$ ,  $P_{\max}$  and  $\eta$  are underestimated (overestimated)

during the forward (backward) voltage sweep, masking the steady state values [3].

These errors prevent an accurate evaluation of performance parameters, especially those sensitive to the region around  $P_{\max}$ , where the hysteresis is most pronounced [1]. A measure for the extent of the hysteresis error is provided by Refs. [4,5]:

$$\epsilon_{\text{hysteresis}} = \frac{P_{\max,\text{bw}} - P_{\max,\text{fw}}}{P_{\max,\text{bw}} + P_{\max,\text{fw}}} \quad (1)$$

This conflict between measurement duration and measurement precision necessitates a reconstruction of the quasi-steady-state (qss) *IV*-characteristics or techniques to avoid its occurrence. Several approaches have been suggested to overcome hysteresis errors. Herman et al. [6] focused on the optimization of the scan time to avoid transient errors from occurring in the first place. Alternatively, the *IV*-curve can be measured using a series of flashes [4] or with extended time in the hysteretic region around  $V_{mpp}$  [7–9]. Lipps [10] suggested a method to use the dark *IV*-curves for correction. Using a combination of forward and backward sweep, Winter et al. [11] investigated the possibility of averaging the currents, concluding that the approach is not feasible for c-Si solar cells due to the asymmetric nature of the error. Methods, that

\* Corresponding author.

E-mail address: [tobias.kemmer@ise.fraunhofer.de](mailto:tobias.kemmer@ise.fraunhofer.de) (T. Kemmer).

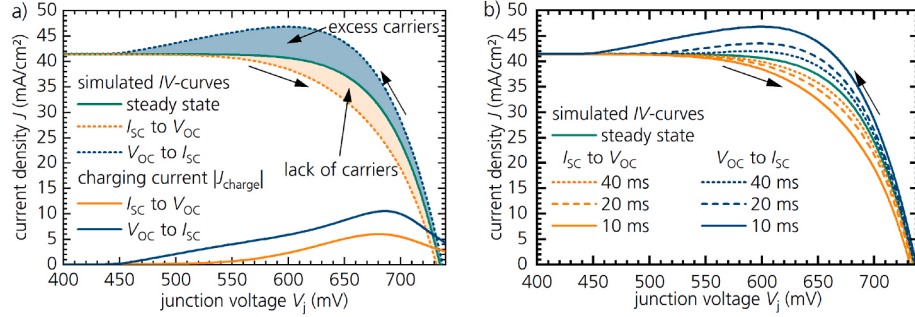


**Fig. 1.** Simulated hysteresis during forward and backward sweep. a) Role of the charging current in raising/decreasing the minority charge carriers during the hysteresis in a 10 ms sweep. b) Dependence of hysteresis on voltage sweep duration in forward and backward direction.

explicitly consider the cell-capacitance [12–15] are more successful in correcting the error but are either proprietary or require extensive fitting procedures. Finally, Sinton et al. [16] derived an analytic correction that can be considered a weighted average of forward and backward sweep based on the charge carrier history using a generalized lifetime and a generalized current density [17,18]. Vahlman et al. [19] discuss the errors associated with this method due to uncertainties in the data acquisition, the determination of the series resistance and numerical inaccuracies in the calculation of derivatives. They further argue, minority carrier lifetime and mobility provide a lower limit for the sweep time.

Besides the parameters commonly extracted from IV-curves, the base doping concentration  $N_B$  can be a valuable parameter to monitor, analyze and model cells or as input parameter for further measurements [20–24]. Techniques have been suggested to extract  $N_B$  from IV-based measurements. Sinton et al. [22] patented a procedure to calculate  $N_B$  by varying the illumination intensity during a step from short circuit condition to maximum power. From this, the change in excess carriers and the base doping concentration are calculated. Ramspeck et al. [21] reported on a technique to calculate  $N_B$  from the hysteresis in IV-curves by comparing the hysteretic forward-IV-curve to the qss-IV-curve. Their approach considers the charging current during the forward sweep to calculate the charge stored in the cell and from this the excess minority carrier density and finally  $N_B$ . However, this method is sensitive to the cell's thickness used in the evaluation and requires a prior reconstruction of the qss-IV-curve.

In this paper, we present in detail a novel approach based on the generalized current density to reconstruct the qss-IV-curve while simultaneously calculating the solar cell's thickness  $d$  and its base doping concentration  $N_B$ . The procedure works solely on IV-data and does not require any additional measurement steps. The proposed procedure thus can also be applied retroactively to already recorded data. In the proposed procedure, the base doping concentration and cell thickness are varied in an optimization procedure to align the generalized current densities of forward and backward sweep. If the curves match, they also correspond to the qss-IV-curve. The combination of  $N_B$  and  $d$  necessary for this correction represents the cell's parameters.

The remainder of the paper is structured as follows: Section 2 covers the theoretical background, discussing the origin of the hysteresis and influences on the transient errors due to experimental details or cell properties. Section 2 also provides a detailed description of our proposed procedure. In Section 3, the experimental details about the solar cells and equipment used for this study are noted. The results of a test batch for system comparison, a SHJ validation batch and a “passivated emitter and rear” cell (PERC, [25]) batch are presented and discussed in Section 4.

## 2. Theory

### 2.1. Origin of hysteresis

During the current-voltage measurement, charges must be redistributed in the material. During a forward sweep ( $I_{sc}$  to  $V_{oc}$ ), minority charge carriers need to be raised, while during a backward sweep ( $V_{oc}$  to  $I_{sc}$ ) the charge carrier density needs to be decreased. For an accurate measurement, the cell and thus the charge distribution should always be in (quasi) steady-state. In the case of very short sweep durations, however, this is no longer given, and the charge carrier density may lag significantly behind. Fig. 1 a) depicts the hysteretic regions in the IV-characteristic highlighting the role of the charge carriers and the charging current.

This effect is commonly represented in equivalent circuit models by a voltage-dependent capacitance consisting of a diffusion and a junction capacitance [3,11]. However, where the hysteresis is most pronounced, primarily the diffusion capacitance is of interest, which can be written as [3]:

$$C_{\text{diff}} = q \frac{n_i^2 L_D}{V_t N_B} \exp\left(b \frac{V_j}{V_t}\right) \quad (2)$$

In this equation  $q$  denotes the elementary charge,  $n_i$  the intrinsic charge carrier density,  $V_j$  the junction voltage,  $L_D$  the minority carrier diffusion length and  $V_t = k_B T/q$  the thermal voltage. In this context,  $b$  is a fitting parameter.

Sinton et al. [16] argue, however, that the cell-capacitance is only an approximation of the true device physics. Instead, the effect of transient errors can be treated by considering the charge carrier history. Assuming a uniform charge distribution in the solar cell throughout its thickness  $d$ , the total charge stored in the cell is given by  $Q = q \cdot d \cdot \Delta n$ . Considering the time-dependent continuity equation [16,17], the total current during measurement can be written as  $J = J_{ss} - \frac{dQ}{dt}$  with the measured current density  $J$  and the steady-state current density  $J_{ss}$ . Thus, a generalized current density can be defined by

$$J_{\text{gen}} = J + q \cdot d \cdot \frac{d\Delta n}{dt} \quad (3)$$

where  $\Delta n$  denotes the excess minority carrier density. The minority carrier density can be calculated to be [16].

$$\Delta n = \sqrt{\frac{N_B^2}{4} + n_i^2 \cdot \exp\left(\frac{V_j}{V_t}\right)} - \frac{N_B}{2} \quad (4)$$

Calculating the time-derivative of Eq. (4), the charge carrier history can be written as

$$\frac{d\Delta n}{dt} = \frac{\partial \Delta n}{\partial V_j} \frac{\partial V_j}{\partial t} = \frac{n_i^2 \cdot \exp\left(\frac{V_j}{V_t}\right)}{V_t \cdot \sqrt{N_B^2 + 4n_i^2 \cdot \exp\left(\frac{V_j}{V_t}\right)}} \frac{\partial V_j}{\partial t} \quad (5)$$

With the knowledge of  $N_B$ ,  $d$ ,  $n_i$  and  $V_j$ , the generalized current density can be calculated using Eqs. (3) and (5). The calculation of  $V_j$  is described later. In the case of the cell's true parameters, the generalized current density is equal to the steady-state current density  $J_{ss}$ . The effect of reduced voltage sweep duration is depicted in Fig. 1 b) for sweep durations of 40 ms, 20 ms and 10 ms. Equation (5) also demonstrates that the extent of the hysteresis is proportional to the time-derivative of the junction voltage.

While the effect of the sweep duration is evident from Eq. (5) and Fig. 1 b), Gao et al. [5] have investigated the influence of additional measurement parameters on the hysteresis of PV modules in greater detail. They conclude that the number of measurement points  $N$  and the hold time  $T_h$  at each step are crucial parameters. At constant  $T_h$ , the transient errors decrease with increasing  $N$ .

From Eqs. (2) and (5), it can further be deduced that a low base doping concentration entails increased transient errors due to the higher base-capacitance. Similarly, both, a high open-circuit voltage and a long minority-carrier diffusion length, will lead to higher diffusion capacitances and thus to an increased hysteresis. Since the diffusion length increases with the minority carrier lifetime  $\tau$ , an increased  $\tau$  also contributes towards hysteresis.

## 2.2. Aligning generalized currents

The proposed procedure to correct the transient errors and to calculate both the base doping concentration  $N_B$  and the cell thickness  $d$  is executed by aligning the generalized currents (combination of Eqs. (3) and (5)):

$$J_{gen} = J_{meas} + q d \frac{n_i^2 \cdot \exp\left(\frac{V_j}{V_t}\right)}{V_t \cdot \sqrt{N_B^2 + 4n_i^2 \cdot \exp\left(\frac{V_j}{V_t}\right)}} \frac{\partial V_j}{\partial t} \quad (6)$$

To this end, the measured IV-data has first to be corrected for influences due to series resistance  $R_s$  and the system's inductance  $L$ . The junction voltage  $V_j$  can be calculated from the measured voltage  $V_{meas}$  by

$$V_j = V_{meas} - JR_s + L \frac{dJ}{dt} \quad (7)$$

Since the system's inductance is not known readily, it must be either assumed or estimated. We chose to estimate the inductance from the measured data. This can be done independently from  $R_s$  by choosing the open-circuit condition, where  $J = 0$  and thus  $V_{j,oc} = V_{oc} + L \cdot \frac{dJ}{dt}$ . Under steady state condition,  $V_{oc}$  is independent of the sweep direction, thus  $V_{ss,oc,fw} = V_{ss,oc,bw} = V_{ss,oc}$ . A first approximation of the inductance can therefore be obtained by assuming equivalent  $V_{j,oc}$  for both sweep directions, resulting in:

$$L_{est} = \frac{V_{oc,fw} - V_{oc,bw}}{\frac{dJ_{bw}}{dt} \Big|_{V_{oc}} - \frac{dJ_{fw}}{dt} \Big|_{V_{oc}}} \quad (8)$$

With the inductance, an interim voltage  $V_L$  removed =  $V_j + L_{est} \frac{dJ}{dt}$  is calculated, which is free of inductive effects, but still affected by series-resistance effects.

As discussed by Pysch et al. [26], several methods to determine the series resistance are available. To minimize the required measurement duration, a method based on already performed measurements is preferable. Ideally, methods such as the  $I_{sc}$ - $V_{oc}$  technique [27] or a multi-light method (MLM) [28] could be used to provide precise results. In our case, however, these would require additional measurements,

which in turn would negate the time-savings from decreasing the sweep duration and thus were not viable for us.

Another aspect, crucial to the determination of  $R_s$ , is the sensitivity of the various possible techniques to hysteresis effects themselves. This is especially important when the illuminated IV-curve has to be evaluated around  $V_{mpp}$ . In that case, the larger the initial hysteresis error is, the further the estimated series resistance might deviate from the actual value. Thus, depending on the extent of the hysteresis error, it can be advisable to choose a theoretically less precise method that is insensitive to hysteresis effects.

Since  $I_{sc}$ - $V_{oc}$ -curve, suns- $V_{oc}$  and MLM curves are not necessarily recorded in our measurement setup, we chose to calculate  $R_s$  according to Aberle et al. [29] by comparing illuminated and dark IV-curves using the correction by Dicker [30], as long as the extent of the hysteresis is limited. Since both curves should be subject to the same hysteresis effects, the influence of the hysteresis around  $V_{mpp}$  on the estimation is expected to be minor. While any pair of IV-curves is conceivable, our implementation uses the illuminated and dark IV-curves in forward direction. For hysteresis errors larger than approx. 12%, the series resistance is estimated by the dark series resistance, described by Ref. [29] which is independent of  $V_{mpp}$ .

With these estimates for  $R_s$  and  $L$ , the junction voltage  $V_j$  can be calculated and used as a basis for the hysteresis analysis. The intrinsic carrier density is calculated self-consistently [31]. With the junction voltage and intrinsic carrier density determined, Eq. (6) has two remaining unknown parameters: the cell thickness  $d$  and base doping concentration  $N_B$ .

The main assumption is now  $J_{gen} = J_{ss}$  for both, forward and backward sweep, for the true values of  $d$  and  $N_B$ . Thus, the generalized currents of forward and backward sweep should also be identical, i.e.  $J_{gen,fw} = J_{gen,bw}$ . The values of  $N_B$  and  $d$  can then be found by using them as optimization parameters in a fit of  $\Delta J_{gen} = J_{gen,fw} - J_{gen,bw}$  to zero over the whole voltage range

$$0 = \Delta J_{gen} = \Delta J_{meas} + q d \frac{n_i^2 \cdot \exp\left(\frac{V_j}{V_t}\right)}{V_t \cdot \sqrt{N_B^2 + 4n_i^2 \cdot \exp\left(\frac{V_j}{V_t}\right)}} \left( \frac{\partial V_{j,fw}}{\partial t} \Big|_{V_j} - \frac{\partial V_{j,bw}}{\partial t} \Big|_{V_j} \right) \quad (9)$$

where  $\Delta J_{meas} = J_{meas,fw} - J_{meas,bw}$ . With the optimized values of  $N_B$  and  $d$ , the generalized currents and thus  $J_{ss}$  can be calculated and the usual evaluation of the IV-characteristics can be performed.

## 2.3. Initial guesses and optimization

The determination of  $N_B$  and  $d$  by minimizing  $\Delta J_{gen}$  has two drawbacks that need to be addressed. Firstly, the two parameters are covariant resulting in suboptimal results and large errors. Secondly, the optimization potentially depends on the initial guess. Both drawbacks can be addressed by making an initial estimation based on the IV-data. Appropriate values for the initial guess can be obtained by using Eq. (9) at only two points  $(V_k, J_k)$  of the IV-curve. Since the resulting system consists of two equations and two unknowns, analytic solutions for  $N_B$  and  $d$  can be calculated:

$$d = \frac{V_t}{q} \sqrt{\frac{n_{i1}^2 \cdot \exp\left(\frac{V_1}{V_t}\right) - n_{i2}^2 \cdot \exp\left(\frac{V_2}{V_t}\right)}{\frac{\Delta \dot{V}_1^2}{\Delta J_1^2} n_{i1}^4 \cdot \exp\left(2 \frac{V_1}{V_t}\right) - \frac{\Delta \dot{V}_2^2}{\Delta J_2^2} n_{i2}^4 \cdot \exp\left(2 \frac{V_2}{V_t}\right)}} \quad (10)$$

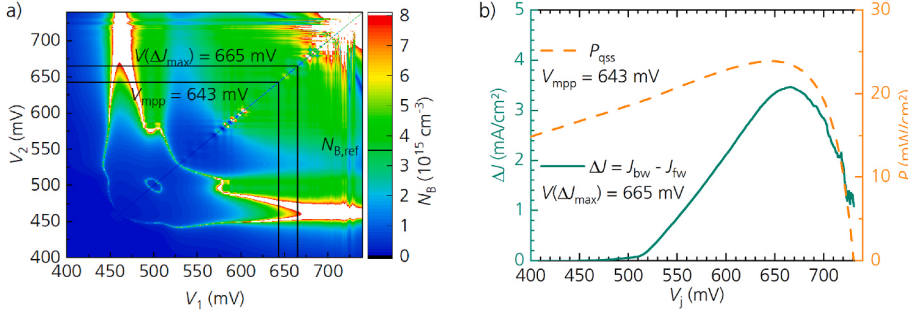


**Fig. 2.** Estimation of initial values for optimization process based on two points of the IV-curve of a cell with  $N_B = 3.39 \cdot 10^{15} \text{ cm}^{-3}$  according to CV-measurements. a) Colormap of  $N_B$  as determined from any possible combination of measured voltages. Blue and black (red and white) areas mark values of  $N_B$  that are too low (high). b) Difference between forward and backward current. (For interpretation of the references to color in this figure legend, the reader is referred to the Web version of this article.)

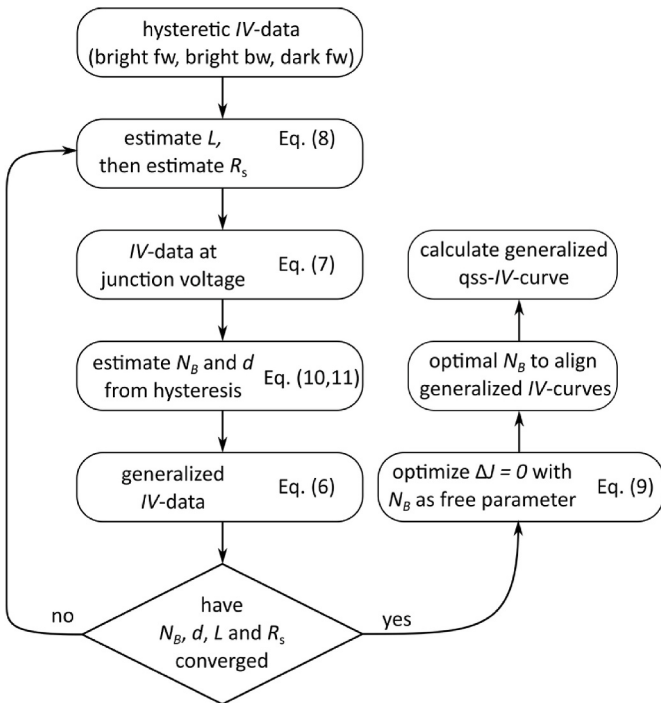


**Fig. 3.** Proposed process flow to reconstruct a qss-IV-characteristics and determine  $N_B$  and  $d$  from hysteretic IV-measurements.

$$N_B = 2n_{i1}n_{i2} \sqrt{\frac{\exp\left(\frac{V_1}{V_t}\right) \Delta \dot{V}_2^2 n_{i2}^2 \cdot \exp\left(2 \frac{V_2}{V_t}\right) - \exp\left(\frac{V_2}{V_t}\right) \Delta \dot{V}_1^2 n_{i1}^2 \cdot \exp\left(2 \frac{V_1}{V_t}\right)}{\Delta \dot{V}_1^2 n_{i1}^4 \cdot \exp\left(2 \frac{V_1}{V_t}\right) - \Delta \dot{V}_2^2 n_{i2}^4 \cdot \exp\left(2 \frac{V_2}{V_t}\right)}} \quad (11)$$

Here shorthands are used to denote  $\Delta \dot{V}_k = \left. \frac{\partial V_{j, fw}}{\partial t} \right|_{V_k} - \left. \frac{\partial V_{j, bw}}{\partial t} \right|_{V_k}$  and  $\Delta J_k = J_{\text{meas}, fw}(V_k) - J_{\text{meas}, bw}(V_k)$ . For optimal results, the choice of  $(V_k, J_k)$  is crucial. It is plausible that Eq. (10) and (11) should be evaluated at positions where the hysteresis is pronounced. This also shows in Fig. 2 a), where the estimated base-doping concentration is shown for pairwise

combinations of junction voltages in a range from 0.4 V to 0.74 V. Fig. 2 b) shows  $\Delta J(V_j)$  and  $P_{qss}(V_j)$  for the same device. The colormap in Fig. 2 a) exhibits a plateau around the maximum of  $\Delta J(V_j)$  and  $V_{mpp}$ . Suitable choices were thus found to be around  $V(\Delta J_{\max})$  or  $V_{mpp}$ , which appears to be positioned more centrally in the plateau. For the analysis in this paper, we chose  $V_1 = V_{mpp}$  and  $V_2 = V_{mpp} - 40 \text{ mV}$ , as we found these values to yield the best results during development.

Based on these initial guesses for  $d$  and  $N_B$ , also a guess for  $J_{\text{gen}}$  can be calculated from Eq. (6). Using these guesses, improved guesses of  $R_s$  (and optionally  $L$ ) and therefore  $V_j$  can be made. Similarly, the calculation of  $n_i$  is repeated. The process can then be repeated until all values have converged, which usually takes less than 10 iterations. To avoid the covariance of  $d$  and  $N_B$ , the optimization of Eq. (9) can be performed using only  $N_B$  as a free parameter, since a reasonable estimate for the cell thickness has already been determined. The overall process, including estimation and improvements is depicted in Fig. 3.

### 3. Experimental

IV-data was measured during a voltage sweep of 30 to 40 ms, in four-wire configuration on an AAA inline flash-tester by h.a.l.m. elektronik GmbH. Their “advanced hysteresis” approach [13] is taken as reference for the basic parameter extraction on the reconstructed qss-IV-curves. For PERC cells the sweep time is reduced to 6 ms to ensure the presence of a hysteresis. We apply the procedure described in section 2 to the previously recorded IV-data. For the iterative estimation of  $N_B$  and  $d$  the IV-curves are evaluated at  $V_1 = V_{mpp}$  and  $V_2 = V_{mpp} - 40 \text{ mV}$ . The optimization is then only performed using  $N_B$  as a free parameter. Additionally, we report the values of an optimization with both  $N_B$  and  $d$  as free parameters.

The proposed procedure was developed using a batch of 29 SHJ cells (batch Dev, 40 ms sweep duration, manufactured at Fraunhofer ISE). Since the results of this batch are prone to overfitting due to repeated use during development, these results will not be discussed in detail.

For the validation of the procedure an unknown test set of 120 SHJ cells (batch A, manufactured at Fraunhofer ISE) was evaluated. These cells were not used during the development of the procedure. Some basic information about the batches is listed in Table 1. Inductive resistivity measurements on the as-cut wafers are used as reference measurements for the determination of the base doping concentration for this batch.

For a system comparison, the procedure was applied to an independent data set (batch B) consisting of another 29 SHJ cells from

**Table 1**

Overview of the solar cell batches that were used in the development (Dev) and the validation (A, B, C; SHJ and PERC) of the proposed procedure.

batch	Type	number of cells	min $N_B$ ( $10^{15} \text{ cm}^{-3}$ )	max $N_B$ ( $10^{15} \text{ cm}^{-3}$ )	min $V_{oc}$ (mV)	max $V_{oc}$ (mV)	min $\eta$ (%)	max $\eta$ (%)
Dev	SHJ	29	2.88	5.54	729.6	734.8	21.8	22.4
A	SHJ	120	3.05	6.67	725.1	737.9	21.7	22.8
B	SHJ	29	1.66	6.29	724.2	735.9	20.4	22.1
C	PERC	180	12.1	32.0	675.7	680.8	22.0	22.4

**Table 2**

RMSD of performance parameters extracted from the reconstructed qss-IV-characteristic compared to the reference values from h.a.l.m. elektronik's "advanced hysteresis" approach. Additionally, the average hysteresis error before ( $\varepsilon_{\text{before}}$ ) and after ( $\varepsilon_{\text{after}}$ ) correction is listed.

RMSD	$\eta$	FF	pFF	$V_{\text{oc}}$	$R_s$	$\varepsilon_{\text{before}}$	$\varepsilon_{\text{after}}$
batch	(%) <sub>abs</sub>	(%) <sub>abs</sub>	(%) <sub>abs</sub>	(mV)	( $\Omega \text{ cm}^2$ )	(%)	(%)
Dev	0.050	0.045	0.37	0.20	0.016	4.44	-0.084
A	0.052	0.08	0.39	0.24	0.028	5.63	-0.10
B	0.10	0.39	0.58	0.58	0.072	6.20	-0.16
C	0.054	0.398	-	2.13	0.024	1.64	0.017

**Table 3**

RMSD of the extended parameters extracted from the hysteresis compared to reference values. For  $N_B$ , CV-measurements or inductive resistivity measurements are used as reference.  $N_{B,\text{opt}}$  denotes the values extracted with the proposed procedure. For  $N_{B,\text{free } d}$ ,  $d$  was used as a free optimization parameter.  $N_{B,\text{Ramspeck}}$  denotes the values calculated by our own implementation of the procedure reported in Ref. [14].  $N_{B,\text{offline}}$  and  $N_{B,\text{inline}}$  are the values reported by the offline (Sinton FCT-450) and the inline flash tester (h.a.l.m. elektronik), respectively.

RMSD	$N_{B,\text{opt}}$	$N_{B,\text{free } d}$	$N_B$	$N_{B,\text{offline}}$	$N_{B,\text{inline}}$	$d$
batch	( $10^{14} \text{ cm}^{-3}$ )	( $\mu\text{m}$ )				
Dev	<b>2.96</b>	9.11	4.27	3.27	-	10.3
A	<b>3.33</b>	26.3	4.12	-	-	23.6
B	<b>6.12</b>	28.9	6.48	6.84	5.6	34.6
C	<b>161</b>	179	121	-	-	105
C (fixed $d$ )	<b>29.7</b>	-	13.9	-	-	-

different sources, including inhouse and industrial cells. For this batch, capacitance-voltage measurements (CV) with an area enhancement factor of 1.09 are used as reference for  $N_B$  [32]. The extracted base doping concentrations of batch B are compared to (i) data measured on a FCT-450 offline flasher from Sinton Instruments, (ii) the procedure

reported by Ramspeck et al. [21] that we calculate parallel to our proposed procedure, and (iii) the values provided by the inline flash-tester used for the IV-measurements. In the case of the FCT-450 flasher, the thickness of the samples was set to 160  $\mu\text{m}$  for all cells. The other procedures use a thickness derived from the hysteresis data.

Finally, the proposed procedure was applied to a batch of approx. 180 PERC cells (batch C) manufactured at Fraunhofer ISE to test the applicability of the proposed procedure on PERC cells. The parameter range of these batches is listed in Table 1, too. For batch C, again inductive resistivity measurements on the as-cut wafers were used as reference measurements for the determination of  $N_B$ .

## 4. Results and discussion

As an overview, the root mean square deviation (RMSD) of the basic parameters extracted from the reconstructed qss-JV-curve is reported in Table 2 compared to the reference measurements for all tested batches. Additionally, the average hysteresis error  $\varepsilon$  before and after reconstruction is noted. Table 3 lists the RMSD for the base doping concentration and the cell thickness compared to their respective reference values.

### 4.1. Sensitivity analysis

Since the system's inductance  $L$  and the series resistance  $R_s$  are only estimated based on the available data, a sensitivity analysis concerning the hysteresis correction and the base doping concentration seems advisable. Using a sample from the development batch, a one-at-a-time sensitivity analysis was conducted, in which inductance and series resistance were systematically varied and thus not subjected to the estimation/optimization process described in section 2. The input parameters were varied over a wide range around the expected values to include extreme deviations from the values determined by our algorithm.

The results of this sensitivity analysis are depicted in Fig. 4. It is found (Fig. 4 a)) that the inductance only has a weak influence on the determination of the base doping concentration. Simultaneously, the

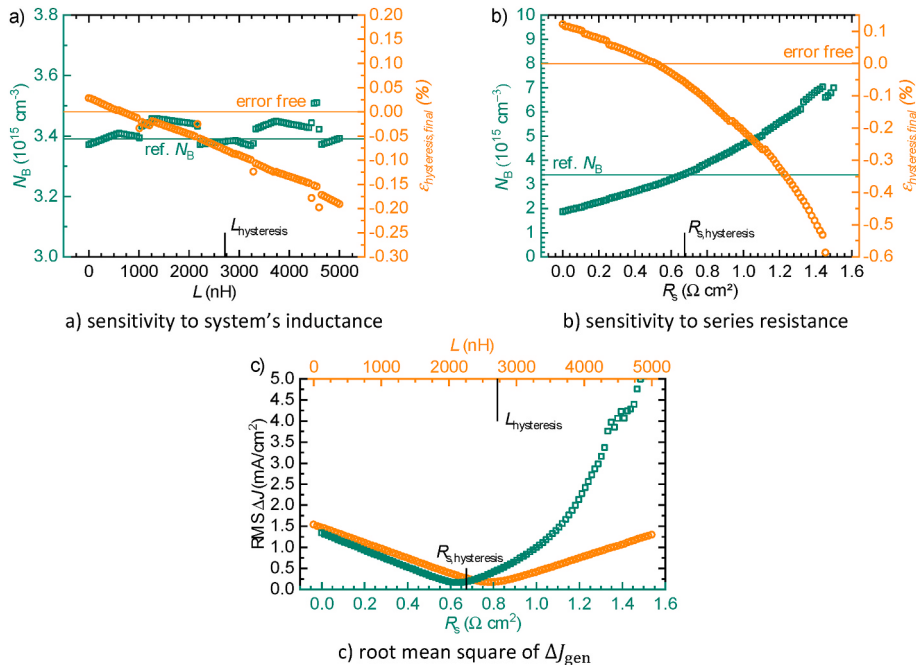


**Fig. 4.** Sensitivity analysis on a SHJ solar cell from batch Dev. The sensitivity of the hysteresis error and the base doping concentration depending on (a) the inductance and (b) the series resistance are analyzed. (c) root mean square of the current difference  $\Delta J_{\text{gen}} = J_{\text{bw,gen}} - J_{\text{fw,gen}}$  of forward and backward generalized IV-curve depending on  $L$  and  $R_s$ .

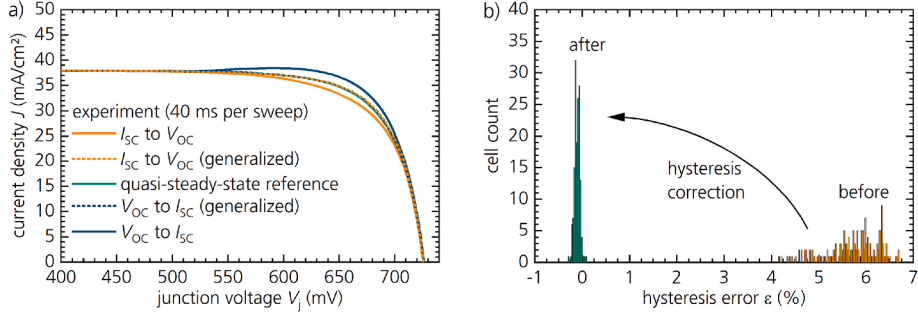


**Fig. 5.** Reconstruction of qss-IV-curve from hysteresis. a) Comparison of uncorrected and corrected (generalized) IV-curves together with reference curve. b) Histogram of hysteresis error before and after the application of the proposed correction procedure.

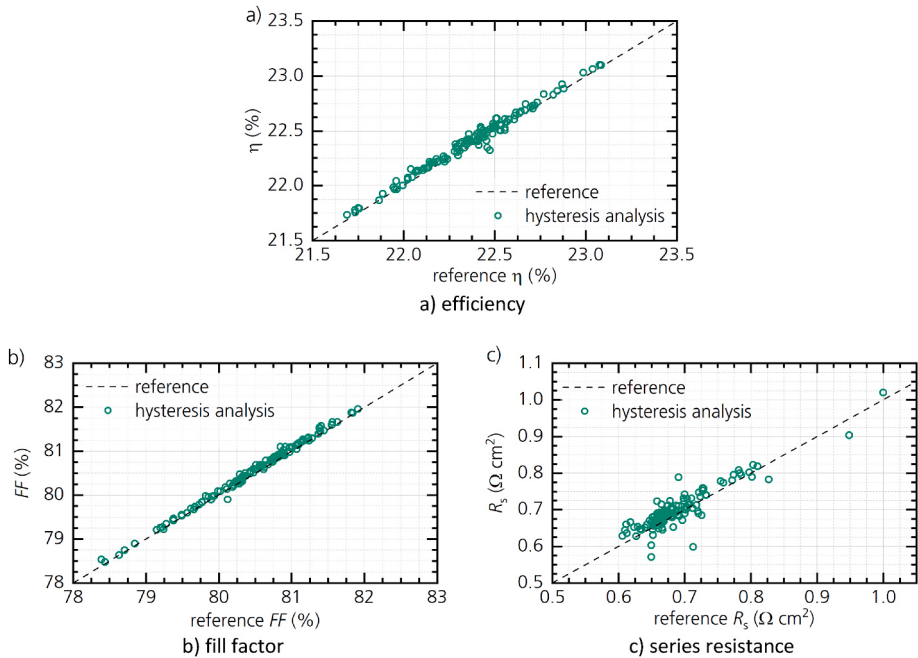


**Fig. 6.** SHJ batch A performance parameters extracted from the reconstructed qss-IV-curves compared to the reference values provided by the “advanced hysteresis” system of the inline tester [13].

hysteresis error shifts towards more negative values, thus leading to an overcompensation of the hysteresis correction at  $V_{mpp}$ . However, the root mean square of  $\Delta J_{gen}$ , i.e. the variable used during optimization, has a minimum at around  $L = 2600$  nH (Fig. 4 c)), indicating the value for optimal overall alignment of the generalized IV-curves. Thus, the inductance presents a trade-off between precision at  $V_{mpp}$  and the overall congruence of the generalized IV-curves, primarily around  $V_{oc}$ .

The series resistance (see Fig. 4 b) and c)) has a more pronounced effect on the determination of the base doping concentration, which shows a monotonous dependence on the series resistance (Fig. 4 b)). RMS  $\Delta J_{gen}(R_s)$  shows a similar trend for low values of  $R_s$  as in the case of the system’s inductance, while an increased RMS  $\Delta J_{gen}$  can be observed for larger values of  $R_s$ . The lower tail of RMS  $\Delta J_{gen}$  can, in fact, be avoided by allowing the inductance to partially compensate for the underestimation of  $R_s$ .

It can be concluded that the overall hysteresis correction is robust concerning the series resistance and the inductance estimation over a reasonable parameter range, while the determination of the base doping concentration is sensitive to series resistance variations it is insensitive to the estimated inductance. This provides also a reference for judging the required precision for the estimation of  $R_s$  and  $L$  in the suggested algorithm.

#### 4.2. SHJ validation batch

The results for the SHJ validation batch A are shown in Figs. 5–7. Fig. 5 a) shows the IV-characteristics of an example solar cell before and after the application of the correction procedure. The generalized curves match the qss-reference curve exceedingly well. The reduction of the hysteresis error across the batch is shown in Fig. 5 b). The average error before correction was  $\epsilon_{\text{before}} = 5.74$  (56) % and after correction  $\epsilon_{\text{after}} = -0.11(7)$  %. Thus, the generalized curves can almost be considered identical. However, it also shows that our procedure slightly overcompensates the hysteresis, same as in the sensitivity analysis. Individual performance parameters (efficiency  $\eta$ , fill factor  $FF$ ,  $P_{max}$  and  $R_s$ ) are plotted in Fig. 6 against their reference values. Overall, the extracted parameters lie close to the identity line, only the series resistance shows some scattering. This could be due to the method used to determine the series resistance and the iterative estimations or an error in the reference data. For the remaining parameters, only individual cells show a considerable deviation from the identity line.

The base doping concentration and base resistivity are depicted in Fig. 7 alongside their reference values. Additionally, the thickness of the cells is shown. The base doping concentration shows a good correlation with the inductively measured values. However, towards higher  $N_B$ , our

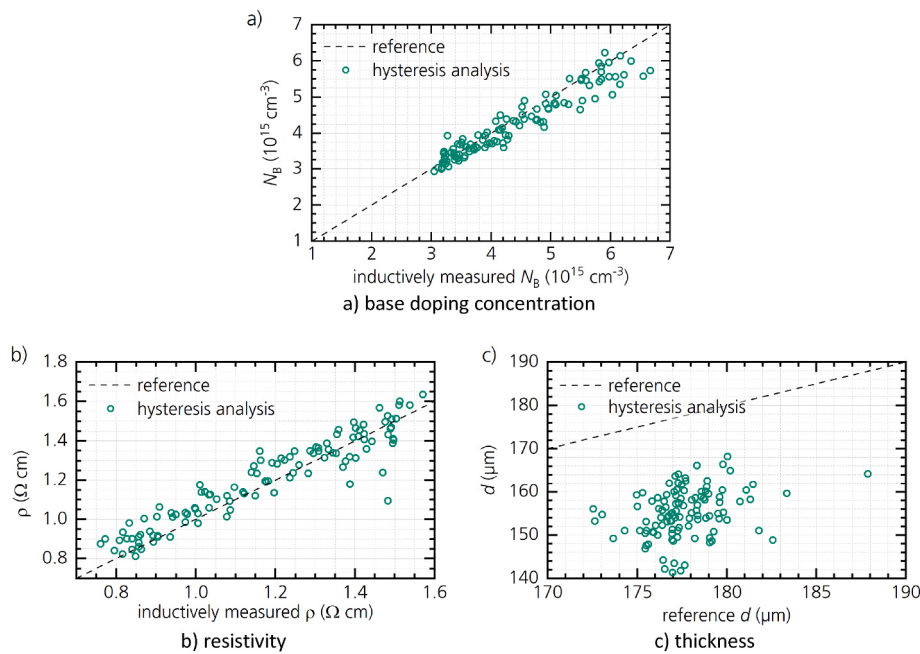


**Fig. 7.** SHJ batch A extended parameters extracted from the reconstructed qss-IV-curves compared to the reference values obtained (a,b) from inductive measurements on the as-cut wafers and (c) from optical thickness measurements at the finished cells, respectively.

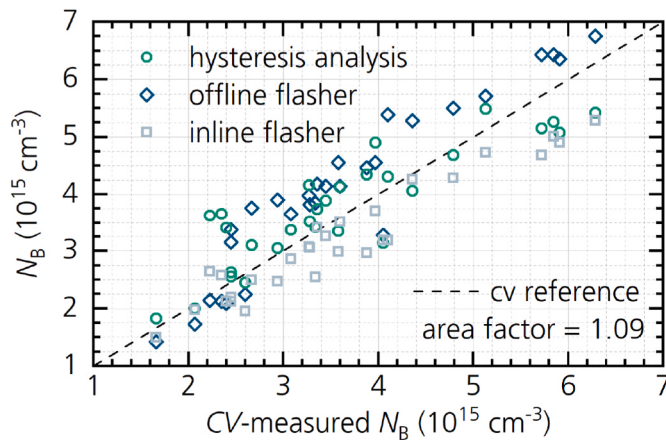


**Fig. 8.** Base doping concentration  $N_B$  according to our proposed procedure (denoted as hysteresis analysis) the FCT-450 offline flasher and the h.a.l.m. elektronik's inline flash-tester with CV-measurements acting as reference values.

procedure tends to result in slightly lower values. For high-resistivity solar cells like SHJ cells, this effect seems to be of minor degree. If this trend continues at higher base doping concentration, this could

prove to be disadvantageous for cells with increased  $N_B$ .

Analogous observations are true for the base resistivity in Fig. 7 b). In general, the extracted data agree well with the reference. At low resistivity, however, the resistivity is slightly overestimated. The thickness in Fig. 7 c) shows much more scattering compared to the optically determined thickness of the inline tester. This is likely due to several reasons. Firstly, due to the optical measurement, the contacts on both sides (contact thickness  $d_{\text{met}} \approx 25 \mu\text{m}$  on front and rear side [33]) are included in the reference measurement while the hysteresis analysis only considers the base thickness. This could explain the systematic deviation of the thickness determined from hysteresis measurements. Secondly, the optically determined reference values reported by the inline tester are subject to uncertainties as well and the cells may exhibit a considerable variation of the thickness over the area. Finally, the thickness in the proposed procedure is estimated based on only two points on the IV-curve. Thus, thickness measurements, while resulting in realistic values, should be considered carefully.

#### 4.3. System comparison

The base doping concentration of the system comparison batch B is plotted in Fig. 8 against CV-measurements with an area enhancement factor of 1.09. Additionally,  $N_{B,\text{offline}}$  measured on the FCT-450 and  $N_{B,\text{inline}}$  are plotted. All procedures show a good correlation with the CV-

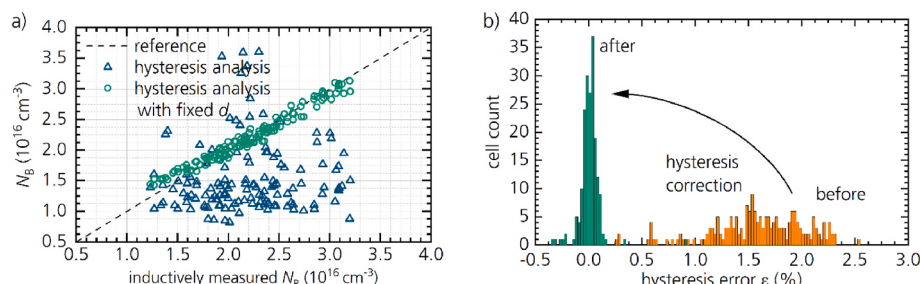


**Fig. 9.** Results of the proposed procedure obtained for the PERC validation batch C. a) Base doping concentration  $N_B$  according to our proposed procedure and our proposed procedure at fixed thickness. b) Hysteresis error before and after application of our proposed procedure.

data. The RMSD of our proposed procedure is around  $6 \cdot 10^{14} \text{ cm}^{-3}$  and thus comparable to procedures in the offline and inline measurement systems. It should be noted that CV-measurements are also prone to uncertainties due to the underlying fit procedure. The data in **Table 3** also highlight how important the estimation of the thickness is to accurately estimate  $N_B$ , as calculations with  $d$  as free optimization parameter result in an increased RMSD.

#### 4.4. PERC validation batch

In the case of the PERC batch C, an analysis of the hysteresis proves much more difficult. Due to the lower resistivity and open-circuit voltage (**Table 1**), the cells are much less prone to showing transient errors in the first place. At 40 ms sweep time, almost no hysteresis is observable ( $|\varepsilon_{\text{before}}| < 0.3\%$ ). Even at 6 ms per sweep ( $|\varepsilon_{\text{before}}| < 2.6\%$ ), the hysteresis is less pronounced than for the SHJ batch.

This also shows in the RMSD in **Table 3**, as the errors for the extracted base doping concentration and thickness are significantly increased. Further tests indicated that this is mainly due to an erroneous estimation of the cell thickness. Based on the hysteresis, the PERC cells are estimated to be around 50  $\mu\text{m}$  thick, which strongly differs from the reference measurements. By assuming a fixed value for the whole batch, the estimates for the base doping concentration could be drastically improved as shown in **Fig. 9 a)**. This, however, only affects the values that are extracted from the hysteresis itself, the extraction of the basic performance parameters yields accurate results without the assumption of a fixed thickness value (**Fig. 9 b)**).

Thus, our proposed method can be used to reduce the voltage sweep duration used for PERC cells down to at least 6 ms and yields the base doping concentration as additional parameter. In fact, we expect improved results for the extraction of the base doping concentration at lower values due to the increased hysteresis.

## 5. Conclusion

We proposed a novel procedure to simultaneously reconstruct the qss-JV-characteristics from hysteretic data and calculate the base doping concentration and cell thickness. The generalized currents of forward and backward sweep are aligned through iterative estimations at two voltages with a final optimization of the base doping concentration. The final generalized currents represent the qss-IV-curve. The procedure requires no external input apart from the JV-data. On the contrary, it can provide  $N_B$  and  $d$  for cell monitoring, cell modelling or as input parameter for further measurements and analyses. The procedure was successfully tested on both SHJ and PERC solar cells. A sensitivity analysis was conducted to analyze the robustness of the procedure concerning the estimation of the system's inductance and the series resistance.

The reconstruction was shown to work reliably on a level comparable with commercially available systems. Parameters extracted from the generalized curves yielded little error compared to a reference system. The calculation of the base doping concentration was found to be comparable to CV-measurements and inductive resistivity measurements with RMSD of around  $6 \cdot 10^{14} \text{ cm}^{-3}$  and less on SHJ test batches. The procedure compares well against an offline- and inline flasher tester and a previously published algorithm.

High resistivity SHJ cells were found to work best with the procedure due to enhanced amount of hysteresis. The analysis of PERC cells is hampered by the little extent of hysteresis effects. We showed that this can be overcome by assuming a realistic value for the cell thickness.

## CRediT authorship contribution statement

**Tobias Kemmer:** Writing – review & editing, Writing – original draft, Visualization, Software, Methodology, Investigation, Formal analysis. **Johannes M. Greulich:** Writing – review & editing, Writing –

original draft, Supervision, Software, Resources, Methodology, Investigation, Funding acquisition, Conceptualization. **Alexander Krieg:** Writing – review & editing, Investigation, Data curation. **Stefan Rein:** Writing – review & editing, Supervision, Project administration, Funding acquisition.

## Declaration of competing interest

The authors declare that they have no known competing financial interests or personal relationships that could have appeared to influence the work reported in this paper.

## Data availability

Data will be made available on request.

## Acknowledgement

This work was supported by the German Federal Ministry for Economic Affairs and Climate Action and by industry partners within the research project “BiZePS-PLUS” under grant number 03EE1064.

## References

- [1] D.L. King, J.M. Gee, B.R. Hansen, Measurement precautions for high-resistivity silicon solar cells, in: Conference Record of the Twentieth IEEE Photovoltaic Specialists Conference, Las Vegas, NV, USA, IEEE, 9/26/1996 - 9/30/1998, 555-559 vol.vol. 1.
- [2] M.Q. Khokhar, S.Q. Hussain, S. Kim, S. Lee, D.P. Pham, Y. Kim, E.-C. Cho, J. Yi, Review of rear emitter silicon heterojunction solar cells, *Trans. Electr. Electron. Mater.* 21 (2020) 138–143, <https://doi.org/10.1007/s42341-020-00172-5>.
- [3] T. Roth, D. Wichmann, K. Meyer, M. Orlob, In-depth analysis of transient errors of inline IV measurements, *Energy Proc.* 8 (2011) 82–87, <https://doi.org/10.1016/j.egypro.2011.06.106>.
- [4] D. Dirnberger, U. Kräling, Uncertainty in PV module measurement—Part I: calibration of crystalline and thin-film modules, *IEEE J. Photovoltaics* 3 (2013) 1016–1026, <https://doi.org/10.1109/JPHOTOV.2013.2260595>.
- [5] Q. Gao, Y. Zhang, Y. Yu, F. Meng, Z. Liu, Effects of I-V measurement parameters on the hysteresis effect and optimization in high-capacitance PV module testing, *IEEE J. Photovoltaics* 8 (2018) 710–718, <https://doi.org/10.1109/JPHOTOV.2018.2810852>.
- [6] M. Herman, M. Jankovec, M. Topić, Optimal I-V curve scan time of solar cells and modules in light of irradiance level, *Int. J. Photoenergy* (2012) 1–11, <https://doi.org/10.1155/2012/151452>, 2012.
- [7] A. Edler, M. Schlemmer, J. Ranzmeyer, R. Harney, Understanding and overcoming the influence of capacitance effects on the measurement of high efficiency silicon solar cells, *Energy Proc.* 27 (2012) 267–272, <https://doi.org/10.1016/j.egypro.2012.07.062>.
- [8] A.S. Eeles, R. Gottschalg, T.R. Betts, Optimising I-V measurements of high capacitance modules using dark impedance measurements, in: IEEE 43rd Photovoltaic Specialists Conference (PVSC), IEEE, Portland, OR, USA, 2016, pp. 3693–3697, 05.06.2016 - 10.06.2016.
- [9] E. Ortega, G. Aranguren, J.C. Jimeno, Photovoltaic modules transient response analysis and correction under a fast characterization system, *Sol. Energy* 221 (2021) 232–242, <https://doi.org/10.1016/j.solener.2021.03.032>.
- [10] F. Lipps, Vergleich und Modellierung von stationär und transient gemessenen I-U Kennlinien an PV-Modulen, Diplomarbeit, Freiburg, 1995.
- [11] S. Winter, J. Metzdorf, Correction procedures for the flasher calibration of PV devices resulting in reduced restrictions and uncertainties, in: 2nd World Conf. On PV Solar Energy Conversion.
- [12] C. Monokroussos, R. Gottschalg, A.N. Tiwari, G. Friesen, D. Chianese, S. Mau, The effects of solar cell capacitance on calibration accuracy when using a flash simulator, in: 2006 IEEE 4th World Conference on Photovoltaic Energy Conference, IEEE, 2006.
- [13] K. Ramspeck, S. Schenk, L. Komp, A. Metz, M. Meixner, Accurate efficiency measurements on very high efficiency silicon solar cells using pulsed light sources, in: 29th European Photovoltaic Solar Energy Conference and Exhibition. Proceedings, 2014, pp. 1253–1256. Amsterdam, The Netherlands.
- [14] G. Friesen, H.A. Ossenbrink, Capacitance effects in high-efficiency cells, *Sol. Energy Mater. Sol. Cell.* 48 (1997) 77–83, [https://doi.org/10.1016/s0927-0248\(97\)00072-x](https://doi.org/10.1016/s0927-0248(97)00072-x).
- [15] D. Hevisov, K. Sporleder, M. Turek, I-V-curve analysis using evolutionary algorithms: hysteresis compensation in fast sun simulator measurements of HJT cells, *Sol. Energy Mater. Sol. Cell.* 238 (2022), 111628, <https://doi.org/10.1016/j.solmat.2022.111628>.
- [16] R.A. Sinton, H.W. Wiltendink, A.L. Blum, Assessing transient measurement errors for high-efficiency silicon solar cells and modules, *IEEE J. Photovoltaics* 7 (2017) 1591–1595, <https://doi.org/10.1109/JPHOTOV.2017.2753200>.

- [17] M.J. Kerr, A. Cuevas, R.A. Sinton, Generalized analysis of quasi-steady-state and transient decay open circuit voltage measurements, *J. Appl. Phys.* 91 (2002) 399, <https://doi.org/10.1063/1.1416134>.
- [18] H. Nagel, C. Berge, A.G. Aberle, Generalized analysis of quasi-steady-state and quasi-transient measurements of carrier lifetimes in semiconductors, *J. Appl. Phys.* 86 (1999) 6218–6221, <https://doi.org/10.1063/1.371633>.
- [19] H. Vahlman, J. Lipping, J. Hyvärinen, A. Tolvanen, S. Hyvärinen, Capacitive effects in high-efficiency solar cells during I-V curve measurement: considerations on error of correction and extraction of minority carrier lifetime, in: 8 pages/35th European Photovoltaic Solar Energy Conference and Exhibition, 2018, pp. 254–261, <https://doi.org/10.4229/35thEUPVSEC20182018-2AO.4.4>.
- [20] R.A. Sinton, A.L. Blum, J. Dinger, W. Dobson, C. Sainsbury, H.W. Wilterdink, Challenges and opportunities in cell and module I-V testing, in: 2018 IEEE 7th World Conference on Photovoltaic Energy Conversion (WCPEC) (A Joint Conference of 45th IEEE PVSC, 28th PVSEC & 34th EU PVSEC), IEEE, 2018.
- [21] K. Ramspeck, Determination of base doping concentration of silicon solar cells from light IV-curves, in: 11th International Conference on Crystalline Silicon Photovoltaics, 2021.
- [22] Ronald A. Sinton, Michael K. Forsyth, Adrienne L. Blum, S. James, Swirhun (BEYER LAW GROUP LLP) US 2014/0333319 A1, 2013.
- [23] R.A. Sinton, A. Cuevas, A quasi-steady-state open-circuit voltage method for solar cell characterization, in: 16th European Photovoltaic Solar Energy Conference.
- [24] K. Dapprich, R.A. Sinton, H.W. Wilterdink, W. Dobson, C. Sainsbury, J. Dinger, Using doping variation to determine J<sub>0</sub>s at I-V test, in: 11th International Conference on Crystalline Silicon Photovoltaics, 2021.
- [25] A.W. Blakers, A. Wang, A.M. Milne, J. Zhao, M.A. Green, 22.8% efficient silicon solar cell, *Appl. Phys. Lett.* 55 (1989) 1363–1365, <https://doi.org/10.1063/1.101596>.
- [26] D. Pysch, A. Mette, S.W. Glunz, A review and comparison of different methods to determine the series resistance of solar cells, *Sol. Energy Mater. Sol. Cell.* 91 (2007) 1698–1706, <https://doi.org/10.1016/j.solmat.2007.05.026>.
- [27] M. Wolf, H. Rauschenbach, Series resistance effects on solar cell measurements, *Adv. Energy Convers.* 3 (1963) 455–479, [https://doi.org/10.1016/0365-1789\(63\)90063-8](https://doi.org/10.1016/0365-1789(63)90063-8).
- [28] K.C. Fong, K.R. McIntosh, A.W. Blakers, Accurate series resistance measurement of solar cells, *Prog. Photovoltaics Res. Appl.* 21 (2013) 490–499, <https://doi.org/10.1002/pip.1216>.
- [29] A.G. Aberle, S.R. Wenham, M.A. Green, A new method for accurate measurements of the lumped series resistance of solar cells, in: 23rd IEEE Photovoltaic Specialists Conference (PVSC), Conference Record, Louisville, KY, USA, 1993, pp. 133–139.
- [30] J. Dicker, Analyse und Simulation von hocheffizienten Silizium-Solarzellenstrukturen für industrielle Fertigungstechniken, Dissertation, Konstanz, 2003.
- [31] A. Kimmerle, Diffused Surfaces for High Efficiency Silicon Solar Cells, Dissertation, Freiburg, Germany, 2015.
- [32] J. Hilibrand, R.D. Gold, Determination of the impurity distribution in junction diodes from capacitance-voltage measurements, in: S.M. Sze (Ed.), *Semiconductor Devices: Pioneering Papers*, WORLD SCIENTIFIC, 1991, pp. 191–198.
- [33] K. Gensowski, A. Jimenez, S. Tepner, E. Bujnoch, K. Muramatsu, M. Pospischil, F. Clement, Dispensing of low-temperature silver pastes, in: Proceedings of the 9th Workshop on Metallization and Interconnection for Crystalline Silicon Solar Cells, Genk, Belgium, AIP Publishing, 2021, 20007.